Journal of Molecular Liquids 197 (2014) 226–235

Contents lists available at ScienceDirect

Journal of Molecular Liquids

journal homepage: www.elsevier.com/locate/molliq

Bent shaped H-bonded mesogens derived from 1, 5-bis (4-hydroxyphenyl) penta-1, 4-dien-3-one: Synthesis, photophysical, mesomorphism and computational studies

Manoj Kr. Paul *, Popita Paul, Sandip Kumar Saha, Sudip Choudhury

Department of Chemistry, Assam University, Silchar, India

ARTICLE INFO

Article history:
Received 10 December 2013
Received in revised form 30 April 2014
Accepted 7 May 2014
Available online 28 May 2014

Keywords:
Mesogens
H-bonded mesogens
Nematic phase
Fluorescence
DFT studies

ABSTRACT

The synthesis, characterization, photophysical and mesomorphism of new hydrogen bonded (H-bonded) bent shaped mesogens derived from 1, 5-bis (4-hydroxyphenyl) penta-1, 4-dien-3-one are reported. The H-bonded bent shaped mesogens are formed by the complexation of 1: 2 molar ratio of 1, 5-bis (4-hydroxyphenyl) penta-1, 4-dien-3-one as bending unit and polar nitrile terminated ligands containing different linking groups (viz., imine (–CH═N–), azo (–N═N–), ester (–COO–)) as side wing. The transition temperatures and phase characterization have been investigated by differential scanning calorimetry and polarized optical microscopy. The bent core unit is fluorescent and non-mesogenic, whereas, all the nitrile terminated polar ligands are non-fluorescent and displayed enantiotropic smectic A phase. The H-bonded complexes are fluorescent and mesogenic. Nematic phase is induced in two H-bonded complexes whereas one of the H-bonded complexes displayed unidentified B_x phase. The computation studies are performed to obtain optimized stable molecular structures of the compounds, to investigate their electronic transitions and compared with experimental results.

1. Introduction

Hydrogen bonding is an important non-covalent interaction in polar fluids [1] (viz., water), in biological systems (viz., DNA, amino acids etc.) and in mesogen formation [2]. Recently, H-bonding is defined as "*The hydrogen bond is an attractive interaction between a hydrogen atom from a molecule or a molecular fragment X–H in which X is more electronegative than H, and an atom or a group of atoms in the same or a different molecule, in which there is evidence of bond formation*" [3]. Mesogens are considered as complex soft matter due to various molecular interactions and forces involved in the formation of mesophases. H-bonding is one of the typical non-covalent molecular interactions responsible for the organization of molecules in mesogens. This molecular interaction in mesogens could be introduced in two general ways: i) by the introduction of appropriate functional groups, e.g., hydroxyl group or amide groups in the ortho position to an azomethine group; ii) through the complexation of two different components, in which one plays the role of a H-donor (e.g., a carboxylic acid) and the other acts as a H-acceptor (e.g., pyridine derivatives). H-bonding in a liquid crystal generates great interest for basic research to understand the interesting functional properties (viz., chirality) and structures (viz., helicity). However, H-bonding between the mesogens and the dissolved dichroic dye is able to enhance the performance of the liquid crystal displays (LCDs) [4]. In the past few decades, the application of the H-bonding in the formation of the mesogenic materials has been rapidly developed and opened new area of "supramolecular mesogens" [5–7]. Supramolecular mesogens are molecular complexes generated from the complexation of the molecular species (H-atom donor and H-acceptor species) through H-bonding interactions. The H-atom donor and acceptor species may be either mesogenic or non-mesogenic which leads to the formation of a supramolecular mesogens. The mesogenic properties and stabilities of supramolecular mesogens can be modified by different nature of proton donors and acceptors and the position of the H-bonding unit within the supramolecular aggregates [8]. Therefore, over past few decades, different H-donors and acceptors moieties have been explored to generate and stabilize new mesogenic phases [9–14]. Most of the H-bonded mesogens studied are based on the rod-like intermolecular H-bonding [15–19]. The discovery of the polar order and macroscopic chirality in an achiral bent core mesogens has attracted the attention of researchers. Recently, a few reports have been published, which described bent shaped compound possessing intra-or inter molecular hydrogen bonding. The intra-molecular H-bond is formed between the H-atom of the hydroxyl group and N-atom of the imine linkage which, in turn, promotes the stability of the imine linkage and the generation of the new mesophases [20–23]. The intermolecular H-bonding appeared in different combination of H-donor (e.g., derivative of the carboxylic acid) with H-acceptor (e.g., derivative of the pyridine). In 1992, Kato et al. reported first H-bonded bent core mesogen, originated from the interaction of pthalic acid or isopthalic

* Corresponding author. Tel.: +91 3842270879.
E-mail address: paulmanojaus@gmail.com (M.K. Paul).

http://dx.doi.org/10.1016/j.molliq.2014.05.007
0167-7322/

acids (H-donors) with stilbazole derivatives (H-acceptors) [24] as shown in Fig. 1a. Recently, Gimeno et al. have reported new bent shaped H-bonded complexes of stilbazole derivatives and carboxylic acids, which act as H-acceptors and H-donors respectively shown in Fig. 1b–d exhibiting B_2 phase characterized by its tilted lamellar and polar packing [25]. Chen et al. have reported new H-bonded bent-core mesogens bearing a flexible carbosilane chain exhibiting only $SmCP_A$ mesophase [26] whereas branched terminal siloxane unit displaying tilt smectic (SmC_G) phases with highly ordered layer structures [27] as presented in Fig. 1e and f. Recently, mesogenic H-bonded supramolecular complexes were prepared by non-mesogenic proton donor isophthalic acid and mesogenic proton acceptor is a pyridine-based derivative having different terminal groups as presented in Fig. 1g. The complexes display nematic (N) and smectic A (SmA) phases [28,29]. Lin et al. have reported photo-luminescent hydrogen-bonded liquid crystalline trimers constructed by the complexation of two complementary components containing various bi-functional photoluminescent acceptor cores and mono-functional proton donors (in a 1:2 molar ratio) exhibiting N, SmA, SmC and SmX phases [30]. Moreover, Barbera et al. have reported [31] columnar liquid crystalline organizations which arise from non-covalent interactions between melamine derivative and banana-like molecules. Shi et al. reported that bent core H-bonded molecules enhance the stability of the blue phase due to the configuration and molecular structure of bent shaped H-bonded molecules [32]. 1, 5-Bis- (4-hydroxyphenyl) penta-1, 4-dien-3-one is widely used for the biological activities [33] and nonlinear optical materials [34]. To the best of our knowledge, 1, 5-bis- (4-hydroxyphenyl) penta-1, 4-dien-3-one has not been used as the bent core unit for the bent core mesogens. This new bent core unit has been chosen due to its dipole moment along carbonyl group and extended π-conjugation. Moreover, the bent core is fluorescent, non-mesogenic and H-atom donor. In this article, we report synthesis, characterization, mesomorphism and computational studies of new H-bonded bent shaped mesogens.

2. Experimental details

2.1. Materials

All the chemicals were procured from Aldrich (USA), Tokyo Kasei (Japan), and E-Merck (Germany) and have been used without further purification. The solvents used (viz., acetone, ethanol, chloroform, hexane, pyridine, acetonitrile, dichloromethane) are purified by standard procedure well documented in literature. Silica gel G [E-Merck]

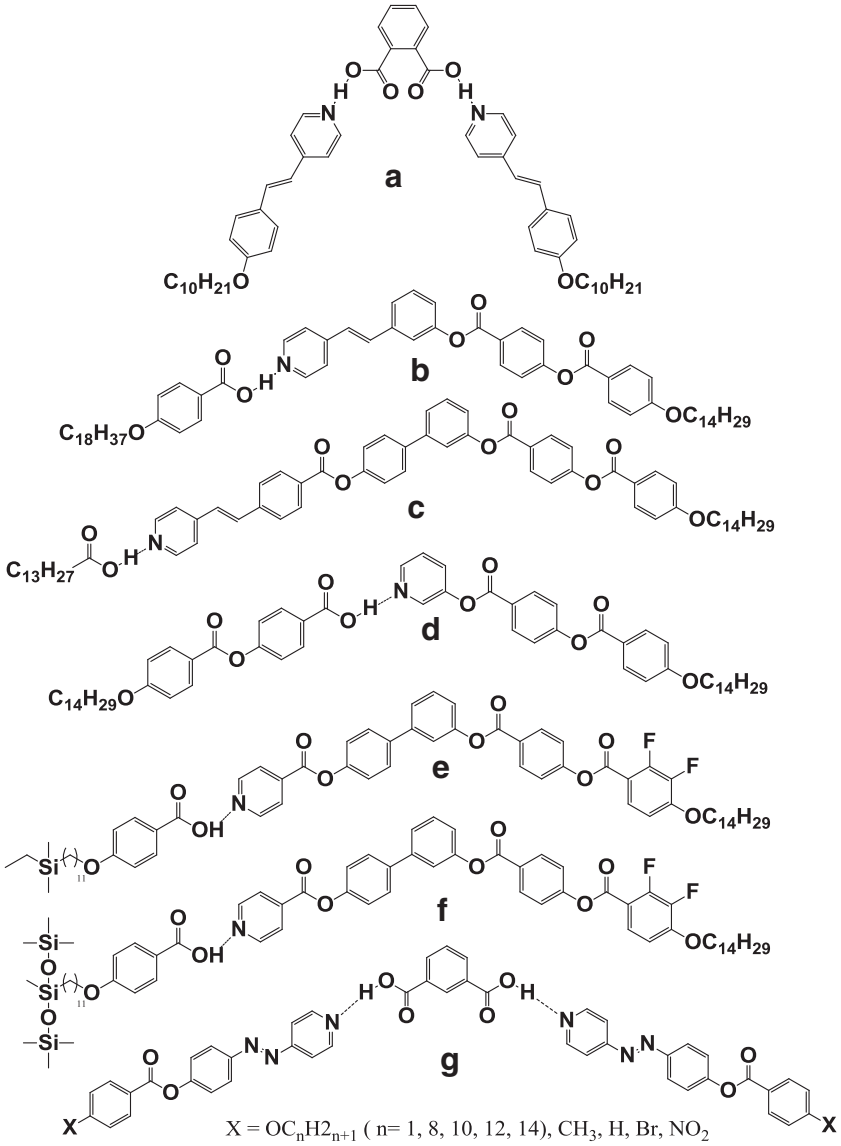

Fig. 1. Few H-bonded bent shaped molecules reported in literature.

was used for thin layer chromatography (TLC). Silica (60–120 mesh) Spectrochem was used for column chromatographic separation and silica gel G (E-Merck, India for TLC). Infrared spectra were recorded on a Shimadzu spectrometer IR Prestige 21 (ν_{max} in cm^{-1}) using a KBr disk. The ^1H nuclear magnetic resonance spectra were recorded on either a JEOL AL300 FT NMR multinuclear spectrometer or Bruker DPX-400 spectrometer in DMSO-d6 or $CDCl_3$ (chemical shift δ in parts per million) solution with TMS as internal standard. Micro analysis of C, H and N elements was determined on a Perkin Elmer 2400 elemental analyzer. UV–visible absorption spectra of the compounds in methanol at 1×10^{-5} M concentration were recorded on a Shimadzu UV-1601PC spectrophotometer (λ_{max} in nm). Fluorescence spectra were recorded with a Shimadzu RF-5301PC spectrofluorimeter with a 150 W xenon lamp as the excitation source. The phase transition temperatures, associated enthalpies and entropies during phase transition were recorded using differential scanning calorimetry (DSC) (Perkin-Elmer Pyris-1 system). The mesogenic properties exhibited by the ligands and H-bonded complexes were observed and characterized by using a polarizing microscope (Nikon Optiphot-2-pol) attached with hot stage (HCS302) and with temperature controller (STC200 from INSTEC Inc. USA).

2.2. Computational details

To study details about the origin of the electronic transitions, the core (***A***), one ligand (***D***) and H-bonded complexes (***A***:***2D***) were computationally analyzed as a representative cases. All calculations were performed with GAUSSIAN 03 package on BRAF supercomputing environment. The geometries of the core, ligand (***D***) and H-bonded complexes (***A***:***2D***) were fully optimized at Becke's three-parameter hybrid exchange functional [35] coupled with the Lee–Yang–Parr nonlocal correlation functional (B3LYP) [36] density functional level of theory using 6-311++g(d,p). The electronic transitions of the compounds were studied computationally under Time-Dependent Density Functional Theory (TD-DFT) using B3LYP (solvent free) functional. This functional has been reported to provide reasonable estimate of transition energies of different types of compounds [37].

2.3. Synthesis and molecular structural characterization

The synthetic procedure for the bent core unit, 1, 5-bis (4-hydroxyphenyl) penta-1, 4-dien-3-one (***A***), nitrile terminated ligands *N*-(4-*n*-hexadecyloxysalicylidene)-4′cyanoaniline (***B***), 4-(*n* dodecyloxy) phenylazobenzonitrile (***C***), 4-cyanophenyl-4′-(*n*-dodecyloxy)benzoate (***D***) and their corresponding bent shaped H-bonded complexes are presented in Scheme 1.

2.3.1. Synthesis of 1, 5-bis (4-hydroxyphenyl) penta-1, 4-dien-3-one (A)

20 ml of conc. hydrochloric acid was added to a mixture of 6.1 g (50 mmol) of 4-hydroxybenzaldehyde and 3.09 g (50 mmol) of boric acid (H_3BO_3) in a 250 ml of round bottom flask. The reaction mixture was cooled at room temperature. 2.3 ml (30 mmol) of acetone was added dropwise to this mixture with vigorous stirring at room temperature for 48 h. Then mixture was poured into 500 ml of ice-cold water. The product was filtered, washed with distilled water and dried at room temperature. The resulting compound was recrystallized from methanol to yield yellow compound. Yield: 3.50 g (65%). IR (KBr, cm^{-1}): 3340, 3190 (ν_{O-H}), 1593 ($\nu_{C=O}$), 1593 ($\nu_{C=C}$, alkene), 1280 (ν_{C-O-Ph}), and 1508($\nu_{C=C, ar}$). ^1H NMR (400 MHz, DMSO-d_6): (δ_H) 7.85 (d, 2H, J = 14 Hz, –CH═CH–), 7.61(d, 4H, J = 8.4 Hz, ArH), 7.06 (d, 2H, J = 14 Hz, –CH═CH–), 6.68 (d, 4H, J = 8.0 Hz, ArH), and 5.45 (s, 2H, –OH). Elemental analysis calculated for $C_{17}H_{14}O_3$: C, 76.68; and H, 5.30. Found: C, 76.78 and H, 5.41.

2.3.2. Synthesis of N-(4-n hexadecyloxysalicylidene) − 4 -cyanoaniline (B)

An ethanolic solution of (4-*n*-hexadecyloxy)-2-hydroxybenzaldehyde (0.724 g, 2 mmol) was added to an ethanolic solution of 4-cyanoaniline (0.236 g, 2 mmol). The solution mixture was refluxed with a few drops of glacial acetic acid as catalyst for 3 h to yield the yellow Schiff's base. The precipitate was collected by filtration and recrystallized from absolute ethanol. Yield: 0.75 g (78%). IR (ν_{max}, cm^{-1}, KBr): 3440 (ν_{O-H}, H bonded), 2918 ($\nu_{as(C-H)}$, CH_3– and CH_2–), 2850 ($\nu_{sy(C-H)}$, CH_3– and CH_2–), 2223 (ν_{CN}, nitrile), 1627($\nu_{C=N}$, imine), 1602 ($\nu_{C=C}$, alkene), 1510 ($\nu_{C=C}$, ar), and 1253 (ν_{C-O-Ph}). ^1H NMR (400 MHz, $CDCl_3$): (δ_H) 13.01 (s, 1H, –OH), 8.66 (s, 1H, –CH═N–), 7.73 (d, 2H, J = 8.0 Hz, ArH), 7.65 (d, 2H, J = 8.0 Hz, ArH), 7.54 (d, 2H, J = 8.4 Hz, ArH), 6.52 (d, 1H, J = 7.8 Hz, ArH), 6.50 (d, 1H, J = 7.8 Hz, ArH), 4.06 (t, 2H, J = 7.8 Hz, $-OCH_2-$), 1.79 −1.26 (m, 28H, $-(CH_2)_{14}-$), and 0.89 (t, 3H, J = 6.6 Hz, CH_3–). Elemental analysis calculated for $C_{30}H_{42}N_2O_2$: C, 77.88; H, 9.15; and N, 6.05. Found: C, 78.00; H, 9.21; and N, 6.23.

2.3.3. Synthesis of 4-(n dodecyloxy)phenylazobenzonitrile (C)

To a solution of 30 ml of H_2O containing hydrochloric acid (6.85 ml, 4.4 M, 30 mmol), 4-aminobenzonitrile (1.18 g, 10 mmol) was added slowly to form a clear solution. To the resulting solution, which was stirred and cooled to 0 °C, an aqueous cold solution of $NaNO_2$ (0.76 g, 11 mmol) was added drop wise, maintaining the temperature of the reaction mixture at 0–5 °C, to yield the diazonium chloride. It was subsequently coupled with phenol (0.94 g, 0.01 mmol), which was dissolved in 11.5 ml of aqueous 2 N NaOH (0.92 g, 23 mmol) solution. The reaction mixture was stirred for 1 h at 0–5 °C and then allowed to warm slowly at room temperature with stirring for over 1 h. The resulting yellow precipitate was filtered and washed with H_2O several times. The crude product was dissolved in CH_2Cl_2 and dried over Na_2SO_4. After the removal of the solvent under reduced pressure, the 4-(4 -hydroxy)azobenzonitrile was recrystallized from ethanol to give a single spot on thin layer chromatography. To a suspension of 4-(4 -hydroxy)azobenzonitrile (2.23 g, 10 mmol) in acetonitrile, K_2CO_3 (6.9 g, 50 mmol) and catalytic amount of tetra-*n*-butylammonium bromide (TBAB) were added and refluxed for 10 h after adding 1-bromododecane (2.5 ml, 10 mmol). The mixture was poured into ice-cold water. After the filtration, the crude product was purified by column chromatography (silica gel, eluent as petroleum ether/ethyl acetate, 97:3v/v) followed by recrystallization from ethanol to obtain the pure product as orange solid. Yield: 3.3 g (84%). IR (ν_{max}, cm^{-1}, KBr): 2914 ($\nu_{as(C-H)}$, CH_3– and CH_2–), 2848 ($\nu_{sy(C-H)}$, CH_3– and CH_2–), 2220 (ν_{CN}, nitrile), 1600 ($\nu_{C=C}$, alkene), 1498 ($\nu_{N=N}$), 1581($\nu_{C=C}$, ar), and 1249 (ν_{C-O-Ph}). ^1H NMR (400 MHz, $CDCl_3$): (δ_H) 8.16 (d, 2H, J = 7.8 Hz, ArH), 7.91 (d, 2H, J = 8.0 Hz, ArH), 7.86 (d, 2H, J = 7.8 Hz, ArH), 7.21 (d, 2H, J = 8.0 Hz, ArH), 4.08 (t, 2H, J = 7.8 Hz, $-OCH_2-$), 1.79–1.26 (m, 20H, $-(CH_2)_{10}-$), and 0.91 (t, 3H, 7.6 Hz, CH_3–). Elemental analysis calculated for $C_{25}H_{33}N_3O$: C, 76.69; H, 8.49; and N, 10.73. Found: C, 76.86; H, 8.55; and N, 11.02.

2.3.4. Synthesis of 4-cyanophenyl-4′-(n-dodecyloxy)benzoate (D)

4-*n*-dodecyloxybenzoic acid (3.0 g, 10 mmol) was dissolved in thionyl chloride and refluxed for 2 h. The excess thionyl chloride was removed under reduced pressure and the resulting compound was dried under vacuum. The resulting 4-*n*-docecyloxybenzoyl chloride and 4-hydroxybenzonitrile (1.90 g, 15 mmol) were dissolved in dichloromethane (30 ml), an aqueous solution of K_2CO_3 (2.76 g, 20 mmol) was added. The resulting solution was vigorously stirred for 24 h after adding a catalytic amount of TBAB. After the stirring was complete, the organic layer was separated, washed several times with the alkaline solution and water and dried over anhydrous sodium sulfate. The evaporation of the solvent gives the crude product which was purified by column chromatography (silica gel, eluent petroleum ether/ethyl acetate, 97:3v/v) followed by recrystallization from ethanol to obtain the pure product as white solid. Yield: 3.1 g (79%). IR (ν_{max}, cm^{-1}, KBr): 2918 ($\nu_{as(C-H)}$, CH_3– and CH_2–), 2850 ($\nu_{sy(C-H)}$, CH_3– and

CH_2-), 2223 (ν_{CN}, nitrile), 1741($\nu_{C=O}$, ester), 1602($\nu_{C=C}$, alkene), 1510($\nu_{C=C}$, ar), and 1253(ν_{C-O-Ph}). ^{1}H NMR (400 MHz, $CDCl_3$): (δ_H) 8.13(d, 2H, J = 8.4 Hz, ArH), 7.96 (d, 2H, J = 8.0 Hz, ArH), 7.56 (d, 2H, J = 7.8 Hz, ArH), 7.13 (d, 2H, J = 8.0 Hz, ArH), 4.06 (t, 2H, J = 7.8 Hz, $-OCH_2-$), 1.78–1.23 (m, 20H, $-(CH_2)_{10}-$), and 0.89 (t, 3H, 7.6 Hz, CH_3-). Elemental analysis calculated for $C_{26}H_{33}NO_3$: C,76.62; H, 8.16; and N, 3.44. Found: C, 76.91; H, 8.46; and N, 3.97.

2.3.5. Synthesis of bent shaped H-bonded complexes

The bent shaped H-bonded complexes were prepared by dissolving the precise 1:2 molar proportions of the proton donor 1, 5-bis (4-hydroxyphenyl) penta-1, 4-dien-3-one (***A***) and the proton acceptor ligands (***B***), (***C***), (***D***) in dry pyridine, followed by ultrasonication for 30 min at 50 °C. The resulting mixture was allowed for few days in a vacuum desiccator for the solvent to evaporate slowly to yield the desired H-bonded bent shaped complexes, (***A***:***2B***), (***A***:***2C***) and (***A***:***2D***) respectively. The synthesis of the H-bonded bent shaped complexes is shown in Scheme 1. The formation of H-bonded complexes was confirmed by thin layer chromatography, elemental analysis and FTIR experiments.

A:2B Yield: 0.56 g (94%). IR (ν_{max}, cm^{-1}, KBr): 3336, 3188 (ν_{O-H}, H-bonded), 2916 ($\nu_{asy(C-H)}$, CH_3- and CH_2-), 2848 ($\nu_{sy(C-H)}$, CH_3- and CH_2-), 2228 (ν_{CN}, nitrile), 1591($\nu_{C=C,}$ aromatic and $-_{CH=N}$, alkene and imine), 1510 ($\nu_{C=C}$, ar), and 1257 (ν_{C-O-Ph}). Elemental analysis calculated for $C_{77}H_{98}N_4O_7$: C, 77.61; H, 8.29; and N, 4.70. Found: C, 78.51; H, 8.58; and N, 5.63.

A:2C Yield: 0.5 g (95%). IR (ν_{max}, cm^{-1}, KBr): 3331, 3190 (ν_{O-H}, H-bonded), 2916 ($\nu_{asy(C-H)}$, CH_3- and CH_2-), 2223 (ν_{CN}, nitrile), 1496 ($\nu_{N=N}$), and 1249 (ν_{C-O-Ph}). Elemental analysis calculated for $C_{67}H_{80}N_6O_5$: C, 76.68; H, 7.68; and N; 8.01. Found: C, 77.25; H, 8.03; and N; 8.89.

A:2D Yield: 0.51 g (94%). IR (ν_{max}, cm^{-1}, KBr): 3338, 3187 (ν_{OH}, H-bonded), 2920 (ν_{as}(C–H), CH_3- and CH_2-), 2850 ($\nu_{sy(C-H)}$, CH_3- and CH_2-), 2231 (ν_{CN}, nitrile), 1734($\nu_{C=O}$, ester), 1602($\nu_{C=C}$, alkene), 1510 ($\nu_{C=C}$, ar), and 1253(ν_{C-O-Ph}). Elemental analysis calculated for $C_{69}H_{80}N_2O_9$: C, 76.64; H, 7.46; and N, 2.59. Found: C, 77.34; H, 8.11; and N, 3.73.

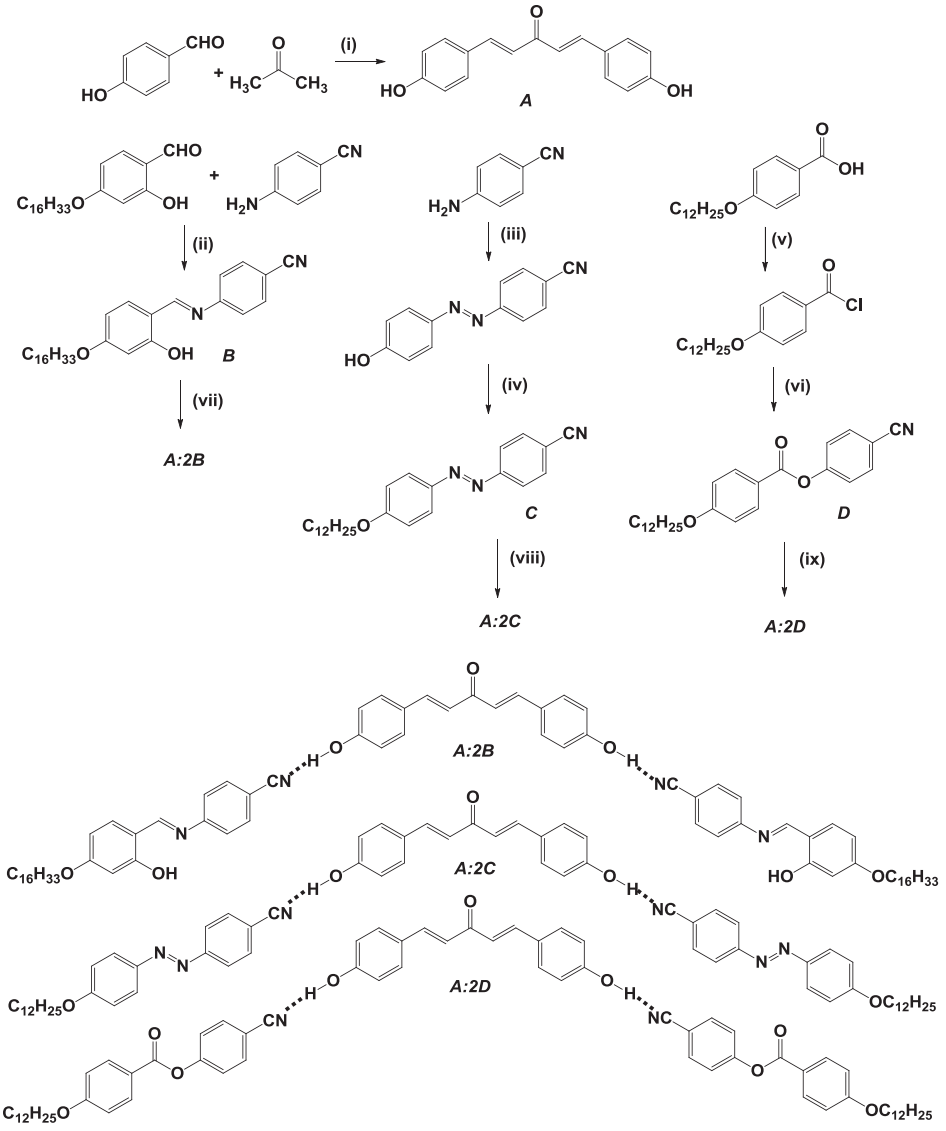

Scheme 1. Synthetic details of compounds ***A***, ***B***, ***C***, ***D***, ***A***:***2B***, ***A***:***2C*** and ***A***:***2D***. Reagents and conditions (i) HCl, H_3BO_3, stirring for 48 h at room temperature; (ii) 2–3 drops glacial acetic acid, EtOH, reflux, 3 h; (iii) aq. HCl, $NaNO_2$, phenol, NaOH; (iv) $C_{12}H_{25}Br$, dry acetonitrile, K_2CO_3, TBAB (catalytic amount), reflux 10 h; (v) $SOCl_2$, Reflux; (vi) 4-cyano phenol, DCM, aq. K_2CO_3, TBAB (catalytic amount), stir for 24 h; (vii) ***A***, Dry Pyridine, ultrasonication for 30 min, 50 °C; (viii) ***A***, Dry Pyridine, ultrasonication for 30 min; (ix) ***A***, Dry Pyridine, ultrasonication for 30 min.

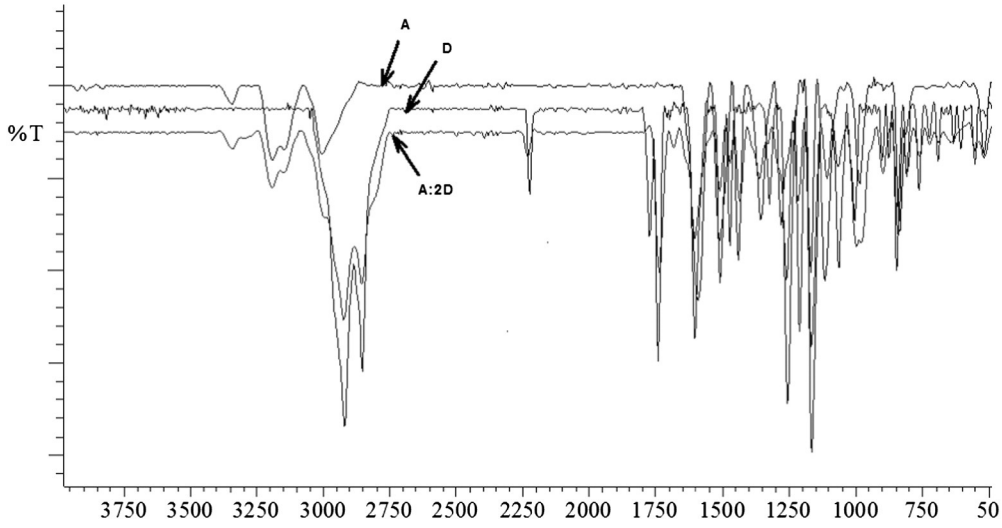

Fig. 2. FTIR spectra of core(***A***), ligand (***D***) and H-bonded complex (***A***:2***D***).

3. Results and discussion

3.1. Synthesis and characterization

The bent core unit (***A***) was synthesized by aldol condensation reaction of 4-hydroxybenzaldehyde with acetone in the presence of boric acid. The formation of the (***A***) was characterized by FTIR. The presence of the band at 1593 cm^{-1} corresponds to aliphatic alkene group (C = C) and further the absence of the band ~1700 cm^{-1} due to the presence of aldehydic group confirms the bent core unit (***A***). The polar nitrile terminated ligands (***B***) were prepared by the condensation of (4-*n*-hexadecyloxy)-2-hydroxybenzaldehyde with 4-cyanoaniline in the presence of a few drops of glacial acetic acid. The compound (***C***) was prepared by diazotization reaction of 4-cyanoaniline followed by the coupling of phenol in basic medium leading to the formation of the intermediate compound, 4-(4/-hydroxy) azobenzonitrile. Further, the etherification of the intermediate compound with *n*-dodecylbromide was carried out by dissolving potassium carbonate in acetonitrile as solvent in the presence of catalytic amount of TBAB. The compound (***D***) was synthesized by converting 4-*n*-alkoxybenzoic acid into 4-*n*-dodecyloxybenzoyl chloride followed by phase transfer reaction of 4-*n*-dodecyloxybenzoylchloride with 4-cyanophenol in the presence of the TBAB. The formation of the linkage in polar terminated ligands was also characterized by IR spectroscopy. The band at 1627 cm^{-1} indicates the formation of the imine group, 1498 cm^{-1} for azo group and 1741 cm^{-1} for ester linkage of the ligands (***B***), (***C***) and (***D***) respectively. The new hydrogen bonded complexes were prepared by dissolving exactly 1:2 molar ratio of protons donor (***A***) with nitrile terminated polar ligands (***B***),(***C***) and (***D***) in dry pyridine followed by slow evaporation of the pyridine in a vacuum desiccator to yield solid compounds. The ultrasonication technique was employed to mixing two components (H-acceptor and H-donor). The solid samples melt, cleanly, without the appearance of the biphasic region indicating the presence of the stoichiometric H-bonded complexes that infer the resulting mixture of the two components is homogenous. The formation of the hydrogen bonding in homogenous complexes was investigated by IR spectroscopy and elemental analysis. The elemental analyses of the compounds were consistent with the proposed molecular formula. The optical studies of the H-bonded complexes were characterized by UV–visible and fluorescence spectroscopy. The thermal and mesomorphic properties of the polar ligands and new H-bonded complexes were determined by polarizing optical microscopy and differential scanning calorimetry.

3.2. FTIR studies

The IR spectra of bent core (***A***), polar ligands (***B***), (***C***), (***D***) and the H-complexes, ***A***:2***B***, ***A***:2***C*** and ***A***:2***D*** were recorded at room temperature in solid KBr. The spectra of representative compounds (***A***), (***D***) and (***A***:2***D***) are presented in Fig. 2 and the spectra of other H-bonded compounds (***A***:2***B*** and ***A***:2***C***) are presented in ESI 1E. The spectra showed a sharp peak ~2224 cm^{-1} for the ν(CN) stretching mode of (***B***), (***C***) and (***D***). The core (***A***) showed a broad peak ~3340 and 3190 cm^{-1} indicates the presence of H-bonded phenolic (OH) group. The infrared absorption frequencies of hydrogen bonded complexes (***A***:2***B***), (***A***:2***C***) and (***A***:2***D***) showed the formation of σ type intermolecular hydrogen bonding between the phenolic (–OH) of (***A***) and the cyano (–CN) group of (***B***), (***C***) and (***D***). On the formation of H-bonding complexes, ν(CN) mode of (***B***), (***C***) and (***D***) shift to higher frequency (i.e. Blue shift) *ca.* 9 cm^{-1} whereas ν(O–H) stretching frequency of core(***A***) shift to lower frequency (i.e. Red shift) is negligibly small (2 ~ 9 cm^{-1}) [38]. The similar shift (~10 cm^{-1}) of the ν(CN) stretching vibration reported when the nitrogen atom of the nitrile group of benzonitrile was complexed with the –OH group of the phenol and however, experimentally no shift was observed in ν(O–H) stretching mode of phenol [39]. Therefore, such system is considered to be a complicated supramolecular system and still a "workhorse" in many laboratories across the world.

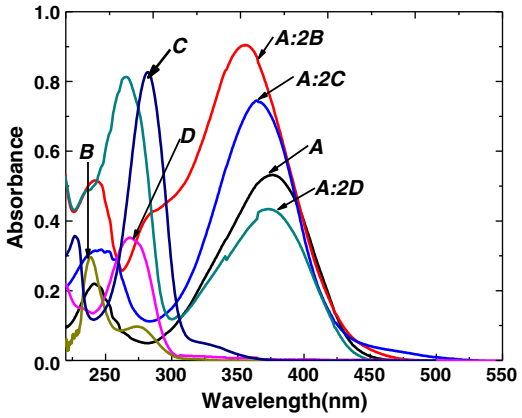

Fig. 3. UV–visible spectrum of core (***A***), polar ligands (***B***), (***C***) and (***D***) and H-bonded complexes (***A***:2***B***), (***A***:2***C***), and (***A***:2***D***) in MeOH (c = 1×10^{-5} M).

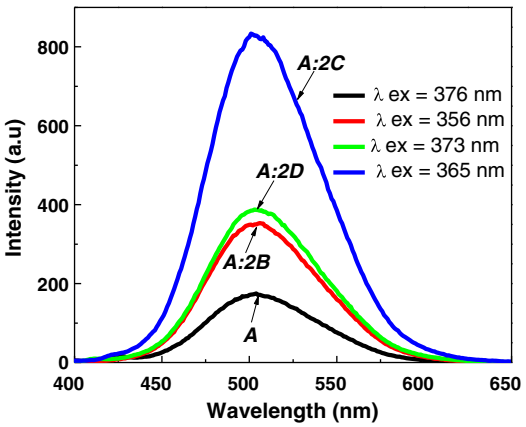

Fig. 4. Fluorescence spectra of core (***A***) and hydrogen bonded complexes (***A*:2*B***), (***A*:2*C***) and (***A*:2*D***) in methanol (c = 1×10^{-5} M) at different excited wavelength.

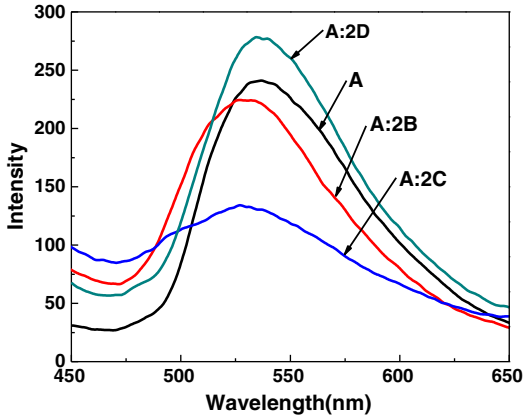

Fig. 5. Fluorescence spectra of core (***A***) and hydrogen bonded complexes in solid state at different excited wavelength.

The examples of such supramolecular system are rare and limited. The change in ν(CN) stretching frequency of nitrile terminated compounds (***B***, ***C*** and ***D***) when complexes with core (***A***) strongly support the formation of σ type hydrogen bonding between triple bond of benonitrile and phenol in the complexes (***A*:2*B***), (***A*:2*C***) and (***A*:2*D***). In the present case, the complex (***A*:2*D***) showed vibrations ~3338 and 3187 cm^{-1}, confirming the stretching of the phenolic – OH group due to intermolecular hydrogen bonding [40] and the peak ~2231 cm^{-1} confirms the stretching mode of the CN group [41].

3.3. Photophysical studies

The UV–visible absorption of H-bond donor (***A***) and H-bond acceptors (***B***), (***C***) and (***D***) and H-bonded complexes (***A*:2*B***), (***A*:2*C***) and (***A*:2*D***) were studied in methanol (MeOH) solvent at 1×10^{-5} M concentration to obtain information regarding absorption maxima as presented in Fig. 3. The absorption maxima of the lowest optical transition were observed 376 nm for core ***A*** (molar extinction coefficient, ε = 53,200 mol L^{-1} cm^{-1}), ~239–282 nm for all the polar ligands (***B***, ***C*** and ***D***) (ε = ~29,000–82,000 mol L^{-1} cm^{-1}) and the H-bonded complexes appear ~356–373 nm (ε = ~43,000–90,000 mol L^{-1} cm^{-1}). These absorption bands with large molar absorption coefficients reflect the π–π* transition of the highly π-conjugated system of the ligands and hydrogen bonded complexes. Interestingly, peak observed ~376 nm for core (***A***) shifted to lower wavelength (Blue shift ~20–3 nm) ~ 356 nm (***A*:2*B***), 365 nm (***A*:2*C***) and 373 nm (***A*:2*D***) indicated the formation of H-bond complexes. The H-bond formation can, also, be rationalized from increase in the absorption intensity. The pattern of H-bond complexes remains the same for all the compounds except ***A*:2*D***. Emission studies on the bent core, polar ligands and H-bonded complexes were carried out in MeOH solution at the concentration of 1×10^{-5} M as presented in Fig. 4. A summary of the photophysical properties of compounds in MeOH is presented in Table 1. The important features are the large Stokes shifted emission ($\Delta\nu_{ss}$) of ~8.26–9.68 eV that was observed and the structure less broad emission band with maxima in the vicinity of ~504 nm. All the neat ligands were non-fluorescent in nature (except B which is weakly fluorescent). The core unit ***A*** shows moderate fluorescence behavior in solution but fluorescence emission intensity increases as on complexation with polar ligands showing the same pattern in all the complexes except ***A*:2*D***. However, the solid thin film, we observed a blue shift (~3–10 nm) indicating decrease in π electron delocalization on H-bond formation which can be due to increase in the energy gap between the highest occupied molecular orbital (HOMO) and lowest unoccupied molecular orbital (LUMO) as presented in Fig. 5. Interestingly,

Table 1
A summary of the photo-physical properties of compounds in MeOH.[a].

Compounds	Abs. λ_{max} (ε)	Fl. λ_{em}	$\Delta\nu_{ss}$
A	241 (22,000)	–	–
	376 (53,200)	504	128 (9.68)
B	274 (9700)	–	–
	239 (29,672)		
C	282 (82,679)	–	–
	350–315 (4100)		
D	269 (35,200)	–	–
A*:2*B	243 (51,600)	–	–
	283 (41,600)	–	–
	356 (90,500)	506	150 (8.26)
A*:2*C	249 (31,000)	–	–
	365 (74,500)	502	137 (9.05)
A*:2*D	265 (81,200)	–	–
	373 (43,400)	503	130 (9.53)

[a] Abs. λ_{max} and Fl. λ_{em} are reported in nm, and the extinction coefficient, ε is calculated in L mol^{-1} cm^{-1}. Stoke shifts ($\Delta\nu_{ss}$) are reported in nm and eV.

Table 2
Mesomorphic phase transition temperatures (T °C), associated enthalpies (Δ*H*, kJ mol^{-1}) and entropy (Δ*S*, J mol^{-1} K^{-1}) for the ligands and H-bonded complexes.

Compounds	Transition	T(°C)	ΔH(kJ mol^{-1})	ΔS (J mol^{-1} K^{-1})	ΔT(°C)
B	Cr-SmA	72.9	70.3	203.2	-
	SmA-Iso	128.7	8.4	20.9	55.8
	Iso-SmA	127.5	7.1	17.7	72.1
	SmA-Cr	56.3	69.4	210.8	-
A*:2*B	Cr1-Cr2	57.2	3.4	10.2	-
	Cr2-Cr3	78.7	14.9	42.5	21.5
	Cr3-B_x	83.5	26.9	68.2	4.8
	B_x-Iso	122.3	7.6	19.2	38.8
	Iso-B_x	121.6	7.4	18.7	65.3
	B_x-Cr	56.3	69.9	212.2	-
C	Cr-Iso	105.8	43.6	115.1	-
	Iso-SmA	104.2	2.3	5.9	19.4
	SmA-Cr2	84.8	13.6	38.0	0.9
	Cr2-Cr1	83.9	23.7	66.5	-
A*:2*C	Cr-Iso	105.9	99.7	263.1	-
	Iso-[N]	105.4[tm]	-	-	2.6
	[N]-SmA	102.8	4.7	12.5	21.2
	SmA-Cr	81.6	102.7	289.6	-
D	Cr1-Cr2	51.8	11.5	35.4	-
	Cr2-SmA	68.8	25.7	75.1	17.0
	SmA-Iso	74.0	2.6	8.9	5.2
	Iso-SmA	73.0	3.1	9.0	22.1
	SmA-Cr2	50.9	25.9	79.9	8.4
	Cr2-Cr1	42.5	8.7	27.5	-
A*:2*D	Cr1-Cr2	58.1	7.3	22.1	-
	Cr2- SmC	68.8	46.6	137.1	10.7
	SmC-Iso	94.3	5.0	13.8	25.5
	Iso-[N]	94.0[tm]	-	-	0.3
	[N]-SmC	93.7	3.3	8.9	40.4
	SmC-Cr	53.3[tm]	-	-	

[tm] indicates POM values. - indicates the Δ*H* and Δ*S* values of the phase transition could not be detected by DSC. [ ] indicates the monotropic phase appears only on cooling.

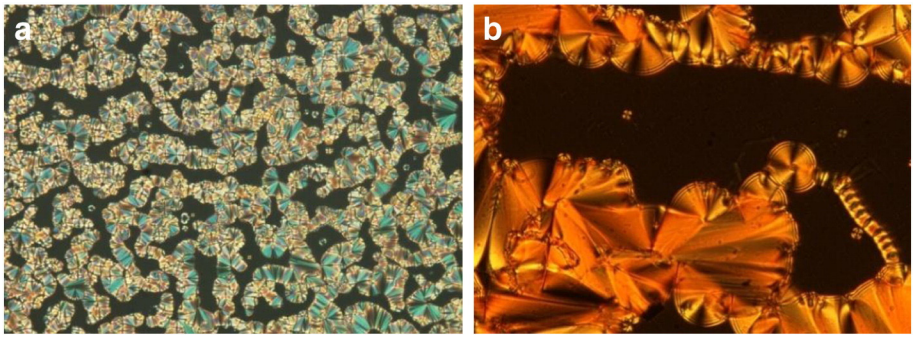

Fig. 6. Polarizing optical microscopic textures of polar ligands (***B***) and (***C***) under crossed polarizer. (a) SmA phase of (***B***) at 127.3 °C, (b) circular focal conic fan texture of SmA with homeotropic region of (***C***) at 86.0 °C.

the fluorescence emission maxima found to be red shifted (~35–23 nm) from methanol solution compared to solid thin film which can be assigned due to the stabilization of conformationally relaxed intermolecular charge transfer (CRICT) state.

3.4. Thermal behavior: differential scanning calorimetry and polarizing optical microscopy

The polarized optical microscopy (POM) was performed to examine the liquid crystalline phases and to confirm the observed phase transition temperatures by POM with the obtained by differential scanning calorimetry (DSC). The liquid crystalline phases, phase transition temperatures, enthalpy and entropy associated with the phase transitions of the ligands and H-bonded complexes are summarized in Table 2. All the compounds exhibited strong birefringence and fluidity in the temperature range characteristic of mesomorphic behavior between the endothermic and exothermic peaks recorded in DSC thermograms in the heating or cooling cycle respectively. All the ligands exhibit mesomorphism.

3.4.1. Ligands

The bent core (***A***) did not exhibit mesophase and melts directly to an isotropic liquid at 165 °C. The H-acceptor polar nitrile terminated ligands (***B***), (***C***) and (***D***) showed mesomorphism. The compounds (***B***) and (***D***) exhibited enantiotropic SmA phase whereas (***C***) displayed monotropic SmA phase. On slow cooling the compound (***B***) from the isotropic liquid, the mesophase is reflected in the form of batonnets at 127.5 °C which further coalesce to give rise to a focal conic fan texture in which large pseudo-isotropic domain occurs due to homeotropic alignment of the molecules indicating the phase as SmA as presented in Fig. 6(a). The sample (***C***) on heating directly melts to isotropic liquid 105.8 °C. On slow cooling the sample (***C***) from the isotropic liquid, a homeotropic circular fan-like texture appears at 104.2 °C which further coalesces to give a focal conic fan texture with large homeotropic region characterizing SmA phase as shown in Fig. 6(b). The sample (***D***) on cooling from the isotropic liquid, the mesophase appeared at 73.0 °C as reflected in the form focal conic fan texture with dark homeotropic region characterizing the phase as SmA. Therefore, all hydrogen acceptor polar nitrile terminated ligands (***B***), (***C***) and (***D***) exhibited SmA phase with large homeotropic (dark) region. The homeotropic region

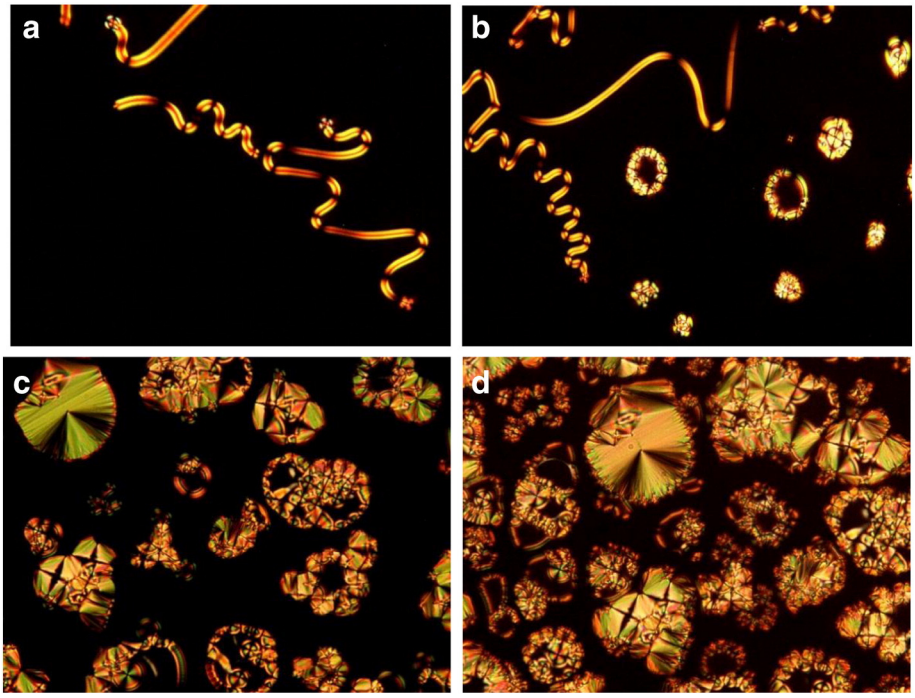

Fig. 7. Optical texture of H-bonded complex, A:2B under crossed polarizers. a) Growth of spiral germ or ribbon like texture from isotropic liquid at 121.4 °C; b) and c) the spiral germ or ribbon texture coalesce to form circular fan-like texture at 120.0 and 115.0 °C respectively; d) more ribbon like textures were grow from the dark region and coalesce to form fan-like texture.

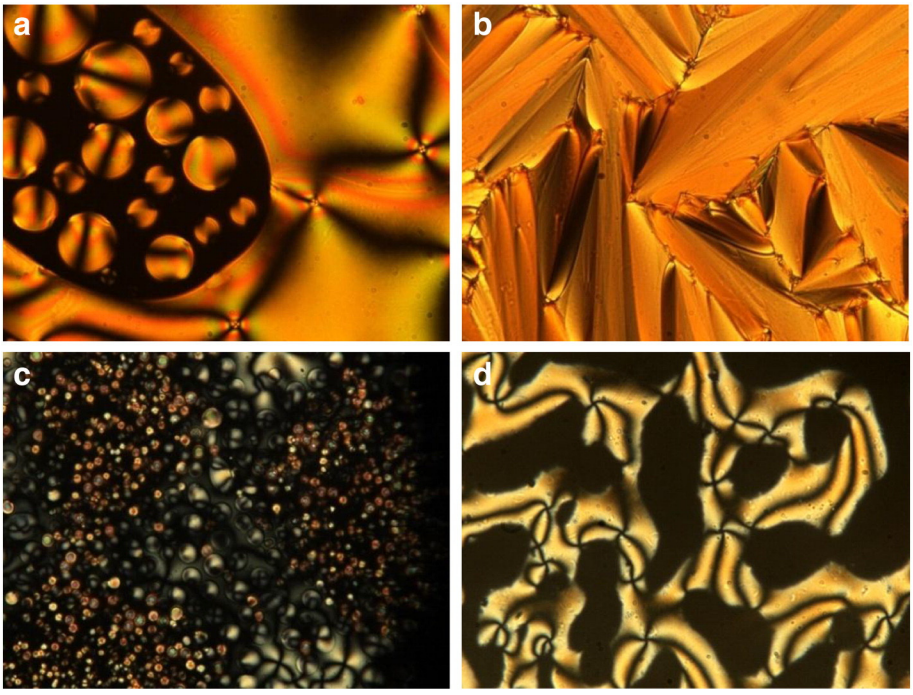

Fig. 8. (a) N droplet of (***A***:2***C***) at 105.4 °C, (b) focal conic fan texture of (***A***:2***C***) 93.0 °C, (c) N droplets of (***A***:2***D***) at 94.0 °C, (d) schlieren texture of (***A***:2***D***) at 93.2 °C.

appears in a mesophase due to the presence of the polar nitrile group present at the end of the terminal position of the ligands. The polar nitrile group stuck to the surface and the hydrocarbon chain pointed on average perpendicular to the substrates [42]. The observed mesophase thermal range (ΔT) of SmA is 72.1 °C for (***B***), 19.4 °C for (***C***) and 22.1 °C for (***D***) respectively. The compound (***B***) exhibited a wide range of the orthogonal SmA phase as compared to compounds (***C***) and (***D***). This is due to the presence of lateral hydroxyl group which promotes stability of phase. Moreover, thermal stability of the (***B***) is higher than (***C***) and (***D***) due to the presence of the lateral hydroxyl group forms an intramolecular H-bonding with imine linkage. The representative DSC thermogram of compound ***D*** is presented in Fig. 9a. The DSC thermogram of the compounds, ***B*** and ***C*** is presented in ESI 2E. Compound ***D*** on heating exhibited three enantiotropic transitions at 51.8 °C with an enthalpy change of 11.5 kJ mol^{-1}, second transition at 68.8 °C with large enthalpy change 25.8 kJ mol^{-1} indicating the crystal to mesophase transition and third transition occurs at 74.0 °C with small enthalpy 2.6 kJ mol^{-1} indicating mesophase to isotropic liquid transition. On slow cooling from isotropic liquid, the compound showed transition at 73.0 °C with small enthalpy change of 3.1 kJ mol^{-1} confirming the isotropic-SmA transition [43]. On further cooling SmA-crystal transition phase is observed at 50.9 °C with a large enthalpy change of 25.9 kJ mol^{-1}. Finally, crystal–crystal transition observed at 42.5 °C with enthalpy change of 8.7 kJ mol^{-1}. The transition temperatures obtained from polarizing optical microscope are in good agreement with the DSC transition temperatures.

3.4.2. H-bonded complexes

The H-bonded complex (***A***:2***B***) on slow cooling from the isotropic melt, a spiral germ like or a ribbon like texture appears at 121.4 °C (Fig. 7(a)) with highly homeotropic dark region and grow (Fig. 7(b)) which on further cooling ribbon like texture coalesces to form a focal conic and fan shaped texture at 120 °C (Fig. 7c–d) with large homeotropic region as presented in a set of microphotograph under crossed polarizers (see Fig. 7). The similar textural behaviors were reported as characteristics of B_7 phase [44]. In this paper, we designated such phase as unidentified B_x phase. The detailed phase characterization by X-ray diffraction and electro-optical measurements is in progress and will be reported elsewhere. The other two H-bonded complexes (***A***:2***C*** and ***A***:2***D***) on cooling the sample from the isotropic liquid, a monotropic nematic (N) phase are induced with SmA or SmC phase. The H-bonded complex (***A***:2***C***) on slow cooling from isotropic liquid, a

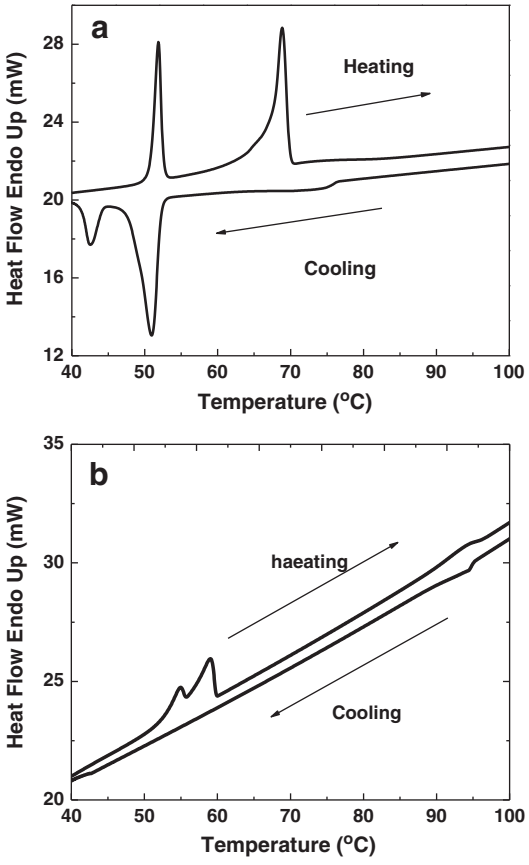

Fig. 9. DSC thermogram a) ligand (***D***); b) H-bonded complex (***A***:2***D***).

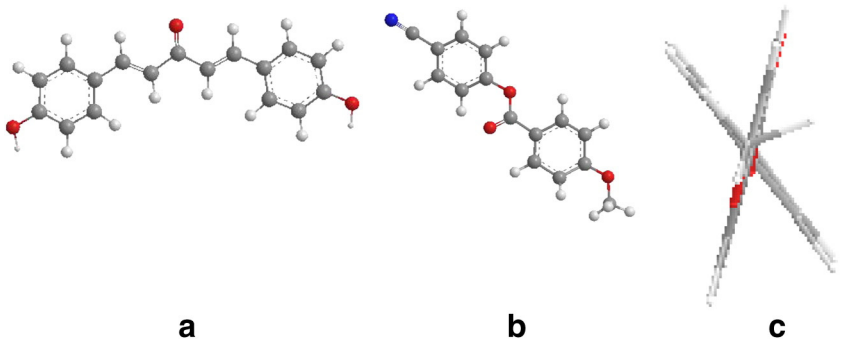

Fig. 10. Optimized structure of (a) core (***A***); (b) Ligand (***D***) and (c) H-bonded complex (***A***: ***2D***).

nematic droplet texture appears at 105.4 °C as presented in Fig. 8a which on further cooling a typical fan-like texture appears at 102.8 indicating SmA phase as presented in Fig. 8b. The H-bonded complex (***A***:***2D***) on slow cooling from isotropic liquid, a nematic droplet texture appears at 94.0 °C as presented in Fig. 8c. On further cooling, the four-brush schlieren texture observed at 93.7 °C indicates SmC phase in Fig. 8d. The thermal range of N phase for (***A***:***2C***) 2.6 °C and 0.3 °C for (***A***:***2D***) respectively, in addition to this mesophase range, the observed SmA mesophase range is 21.2 °C for (***A***:***2C***) and SmC is 40.4 °C for (***A***:***2D***). The representative DSC thermogram of compounds ***A***:***2D*** is presented in Fig. 9b. Compound ***A***:***2D*** on heating exhibited three transitions at 51.8 °C with an enthalpy change of 7.3 kJ mol^{-1}, second transition at 68.8 °C with large enthalpy change 46.6 kJ mol^{-1} indicated the crystal to mesophase transition and third transition occurs at 94.3 °C with small enthalpy 5.0 kJ mol^{-1} indicated mesophase to isotropic liquid transition while on slow cooling only one transition observed at 93.7 °C with enthalpy change 3.3 kJ mol^{-1}. The isotropic to N and SmC to crystal transition were observed by POM but could not observe by DSC. The DSC thermogram of the other H-bonded complexes (***A***:***2B*** and ***A***:***2C***) is presented in ESI 3E. The transition temperatures obtained from polarizing optical microscope are in good agreement with the DSC transition temperatures.

3.5. Computational studies

We performed time-dependent density functional theory (TD-DFT) calculations on models of core (***A***), ligand (***D***) and hydrogen bonded complex (***A***:***2D***) to elucidate the quantum mechanical origins of the UV–visible spectra. The optimized structures of the representative compounds are presented in Fig. 10. The optimized structures show that the core compound maintains planarity in the structure but the two aromatic rings do not maintain co-planarity in the ligand. The rings are at about 50° angled to each other. The TD-DFT computation on the core (***A***) revealed that four bonding orbitals (HOMO, HOMO-1, HOMO-2 and HOMO-3) and two antibonding orbitals (LUMO and LUMO + 1) within the energy band of −1 eV to −8 eV, to be associated in all the transitions probable under UV and visible range. Six transitions were detected within this range, out of which the HOMO → LUMO transition at 386 nm was with the highest oscillator strength followed by HOMO-1 → LUMO + 1 at 271 nm. Other transitions were of very low intensity and merged in within these two peaks. After complexation with the H-bond donor moiety (***D***), there has been considerable changed in the electronic structure of the system as shown in Fig. 11. The TD-DFT study detected only one broad band at 387 nm arising from the HOMO (−5.45 eV) → LUMO +2 (−1.89 eV) transition. The LUMO and LUMO + 1 orbitals degenerate orbitals. Electronic transitions from HOMO → LUMO (and other transitions) were found to be of negligible intensity. Although all the computed results were found to be in very good agreement with the experimental results (see Table 3), the transition corresponding to the higher energy band (266 nm) observed in the experimental study could not be detected in the theoretical studies. The reason could be the complex supramolecular arrangement formed by the real molecules through extensive H-bonding, which could not be replicated in computer.

4. Conclusion

A new bent shaped H-bonded liquid crystal has been synthesized successfully by employing the ultra-sonication technique for mixing two components in an accurate stoichiometry. The three different linking groups (−CH═N−, −N═N−, −COO−) have been used in the mesogenic polar ligand bearing a cyano group at the terminal position which act as H-acceptor in order to understand the structure property relationship on the mesophases. A new non-mesogenic fluorescent

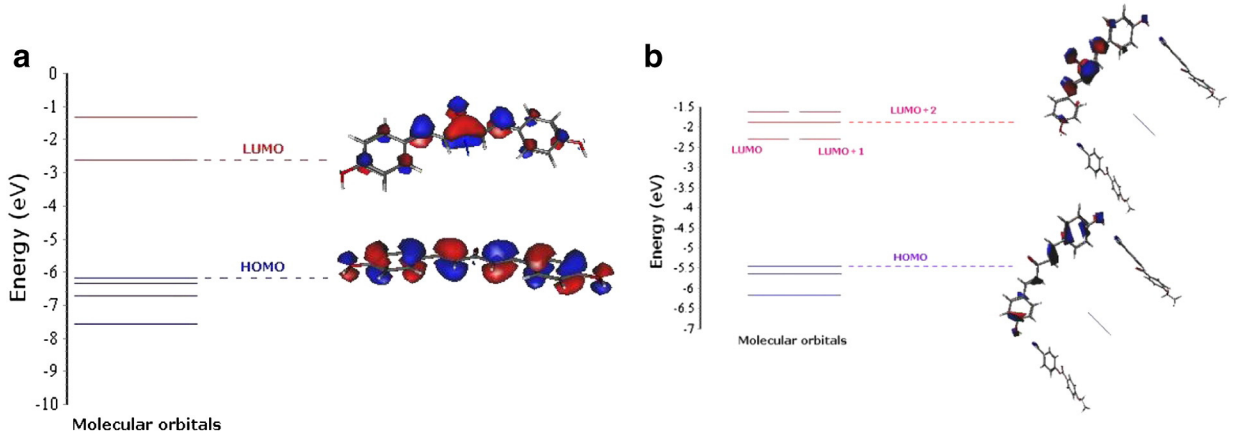

Fig. 11. TD-DFT computed orbital diagram of the (a) core (***A***) and (b) the H-bonded complex (***A***:***2D***) depicting the orbitals found most responsible for the intense electronic transition.

Table 3
Comparison of experimental and theoretical absorption bands.

Compound	Absorption bands (nm)		Electronic transitions
	Experimental	*Theoretical*	
Core (***A***)	242	271	HOMO-1 → LUMO + 1
	377	386	HOMO → LUMO
Complex (***A***:2***D***)	266	–	–
	374	387	LUMO → LUMO + 1

bent core unit is used as an H-atom donor. It is found that the one of the H-bonded complex, (***A***:2***B***) displays wide thermal range of unidentified banana (B_x) phases whereas its polar ligand (***B***) displays enantiotropic SmA phase, a characteristics of the rod shaped mesophase. The H-bonded complexes (***A***: 2***C***) bearing azo linking group exhibits N-SmA phase variants and (***A***:2***D***) contains ester linking group exhibits N-SmC phase variants. Therefore, monotropic nematic phase is induced on complexation. The polar ligand (***C***) and (***D***) exhibits monotropic SmA phase and enantiotropic SmA phase respectively. The bent core unit (***A***) is highly fluorescent. The H-bonded complexes are also fluorescent. The fluorescent responses of H-bonded complexes are ~2–5 times higher than those of the bent core unit (***A***). The H-bonded complexes have large Stoke shift value. The UV–visible absorption of the core and H-bonded complexes are comparable with the theoretical calculation. Therefore, bent core H-bonded compounds are important molecular architectures to generate nematic phase in a bent core system.

Acknowledgment

Authors would like to acknowledge Department of Science and Technology, New Delhi for the financial grant.

Appendix A. Supplementary data

Supplementary data to this article can be found online at http://dx.doi.org/10.1016/j.molliq.2014.05.007.

References

[1] B. Veytsman, J. Phys. Chem. 94 (1990) 8499–8500.
[2] S.I. Torgova, A. Strigazzi, Mol. Cryst. Liq. Cryst. 336 (1999) 229–245.
[3] E. Arunan, G.R. Desiraju, R.A. Klein, J. Sadlej, S. Scheiner, I. Alkorta, D.C. Clary, R.H. Crabtree, J.J. Dannenberg, P. Hobza, H.G. Kjaergaard, A.C. Legon, B. Mennucci, D.J. Nesbitt, Pure Appl. Chem. 83 (2011) 1619–1636.
[4] J. Thote, R.B. Gupta, Ind. Eng. Chem. Res. 42 (2003) 1129–1136.
[5] E.J. Foster, C. Lavigueur, Y.C. Ke, V.E. Williams, J. Mater. Chem. 15 (2005) 4062–4068.
[6] J.M. Lehn, Angew. Chem. Int. Ed. Engl. 27 (1988) 89–112.
[7] T. Kato, J.M.J. Frechet, J. Am. Chem. Soc. 111 (1989) 8533–8534.
[8] R.A. Reddy, C. Tschierske, J. Mater. Chem. 16 (2006) 907–961.
[9] T. Kato, T. Uryu, F. Kaneuchi, C. Jin, J.M.J. Frechet, Liq. Cryst. 14 (1993) 1311–1317.
[10] T. Kato, J.M.J. Frechet, Macromolecules 22 (1989) 3818–3819.
[11] U. Kumar, T. Kato, J.M.J. Frechet, J. Am. Chem. Soc. 114 (1992) 6630–6639.
[12] T. Kato, H. Kihara, T. Uryu, A. Fujishima, J.M.J. Frechet, Macromolecules 25 (1992) 6836–6841.
[13] U. Kumar, J.M.J. Frechet, T. Kato, S. Ujiie, K. Iimura, Angew. Chem. Int. Ed. Engl. 31 (1992) 1531–1533.
[14] U. Kumar, J.M.J. Frechet, Adv. Mater. 4 (1992) 665–667.
[15] M. Paleos, D. Tsiourvas, Angew. Chem. Int. Ed. Engl. 34 (1995) 1696–1711.
[16] M. Paleos, D. Tsiourvis, Liq. Cryst. 28 (2001) 1127–1161.
[17] T. Kato, J.M.J. Frechet, Liq. Cryst. 33 (2006) 1429–1437.
[18] R. Manohar, D. Pal, Shashwati, V.S. Chandel, Z.U. Mazumdar, M.K. Paul, N.V.S. Rao, Mol. Cryst. Liq. Cryst. 552 (2012) 71–82.
[19] K. Wills, J.E. Luckhrust, D.J. Price, J.M. Frechet, H. Kihara, T. Kato, G. Ungar, D.W. Bruce, Liq. Cryst. 21 (1996) 585–587.
[20] N.V.S. Rao, R. Deb, M.K. Paul, T. Francis, Liq. Cryst. 36 (2009) 977–987.
[21] D.M. Walba, E. Korblova, R. Shao, N.A. Clark, J. Mater. Chem. 11 (2001) 2743–2747.
[22] C.V. Yelamaggad, U.S. Hiremath, S.A. Nagamani, D.S.S. Rao, S.K. Prasad, J. Mater. Chem. 11 (2001) 1818–1822.
[23] C.V. Yelamaggad, S. Krishna Prasad, G.G. Nair, I.S. Shashikala, D.S. Shankar Rao, C.V. Lobo, S. Chandrasekhar, Angew. Chem. Int. Ed. 43 (2004) 3429–3432.
[24] T. Kato, H. Adachim, A. Fujishima, J.M. Frechet, Chem. Lett. 21 (1992) 265–268.
[25] N. Gimeno, M.B. Ros, J.L. Serrano, M.R. De la Fuente, Angew. Chem. Int. Ed. 43 (2004) 5235–5238.
[26] W.H. Chen, Y.T. Chang, J.J. Lee, W.T. Chuang, H.C. Lin, Chem. Eur. J. 17 (2011) 13182–13187.
[27] W.H. Chen, W.T. Chuang, U. Jeng, H.S. Sheu, H.C. Lin, J. Am. Chem. Soc. 133 (2011) 15674–156785.
[28] M. Alaasar, C. Tschierske, M. Prehm, Liq. Cryst. 38 (2011) 925–934.
[29] J. Extebarria, M.B. Ros, J. Mater. Chem. 18 (2008) 2919–2926.
[30] H.C. Lin, H.Y. Sheu, C.L. Chang, C. Tsai, J. Mater. Chem. 11 (2001) 2958–2965.
[31] J. Barbera, L. Puig, P. Romero, J.L. Serrano, T. Sierra, J. Am. Chem. Soc. 128 (2006) 4487–4492.
[32] Y. Shi, X. Wang, J. Wei, H. Yang, J. Guo, Soft Matter 9 (2013) 10186–10195.
[33] W.M. Weber, L.A. Hunsaker, S.F. Abcouwer, L.M. Deck, D.L.V. Jagt, Biol. Inorg. Med. Chem. 13 (2005) 3811–3820.
[34] M. Davletbaeva, A.V. Ten'kovtsev, R.A. Bylinkin, V.A. Lukoshkin, V.V. Parfenov, Russ. J. Appl. Chem. 75 (2002) 1537–1538.
[35] A.D. Becke, J. Chem. Phys. 98 (1993) 5648–5652.
[36] C. Lee, W. Yang, R.G. Parr, Phys. Rev. B 37 (1988) 785–789.
[37] D. Jacquemin, E.A. Perpete, G.E. Scuseria, I. Ciofini, C. Adamo, J. Chem. Theory Comput. 4 (2008) 123–135.
[38] M.T. Nguyen, E.S. Kryachko, L.G. Vanquickenbrone, in: Z. Rappoport (Ed.), the Chemistry of Phenols, Wiley, New York, 2002.
[39] S.C. White, H.W. Thompson, Proc. R. Soc. Lond. 291 (1966) 460–468.
[40] S. Kryachko, M.T. Nguyen, J. Phys. Chem. A 106 (2002) 4267–4271.
[41] R.M. Silverstein, G.C. Bassler, T.C. Morrik, Spectroscopic Identification of Organic Compounds, John Wiley and Sons, Singapore, 1991.
[42] D. Demus, J. Goodby, G. W. Gray, H. W. Spiess, V. Vill, Hand book of liquid crystals, ed. by, Vol 2A Willey VCH, Weinheim, 1998.
[43] P.J. Collings, M. Hird, Introduction to Liquid Crystals: Physics and Chemistry, Taylor and Francis, UK, 2009.
[44] M.G. Tamba, U. Baumeister, G. Pelzl, W. Weissflog, Liq. Cryst. 37 (2010) 853–874.